OPTIMAL STRAIN SENSOR PLACEMENT ON AN INSTRUMENTED SUSPENSION FOR TMR SUPPRESSION IN HARD DISK DRIVES

Hany M. Gross and David B. Bogy
Computer Mechanics Laboratory
Department of Mechanical Engineering
University of California, Berkeley
Berkeley, CA 94720

Abstract

The magnetic storage industry has been witnessing a sharp rate of growth of areal recording density, which implies a corresponding growth in both track density and linear bit density. A higher track density, however, imposes a matching reduction in the allowable track misregistration budget. On the other hand, increased spindle rotation speeds are resulting in higher sources of vibration in disk drives, primarily air turbulence excitation. With such meager allowable TMR budgets and elevated windage excitation levels, it is becoming increasingly more difficult for the servo control to maintain the required precise positioning of the ever-smaller giant magneto-resistive heads to read and write data.

The use of strain sensors for active vibration control in disk drives was proposed by several researchers. The basic idea is to strategically attach strain sensors to measure localized strains at key locations on drive structures, so that the sensors will effectively detect structural vibrations that may result in slider off-track motion. The measured strain information can then be used by the controller to suppress slider off-track motion. One of the main tasks in implementing such a strategy is determining the optimal placement of the strain sensors. In this study, the optimal location and orientation of strain sensors on an instrumented suspension was determined based on the degree of observability of modes that contribute to slider off-track motion.

Table of Contents

List of Tables

List of Figures

1. Introduction

The magnetic storage industry has been witnessing a sharp rate of growth of areal recording density. This growth of areal density implies a corresponding growth in both track density and linear bit cell density. The national storage industry consortium (NSIC) recording areal density goal of 100 Gbit/in^2, with a corresponding track density of 175,000 tracks per inch (or 175 kTPI), is no longer a pre-competitive research objective. It has recently been relabeled by the NSIC as 'competitive' material, and is currently making its way into industry roadmaps. It is estimated that track densities greater than 500 kTPI will be necessary to achieve the NSIC new goal of 1Tbit/in^2. This translates into a track pitch of less than 50 nm, and consequently a reduced allowable track misregistration (TMR) budget of less than 5 nm. In addition, increased spindle rotation speeds are resulting in higher sources of vibration in the drive, primarily air turbulence excitation. With such meager allowable TMR budgets and elevated windage excitations, it is becoming increasingly more difficult for the servo controller to maintain the required precise positioning of the ever-smaller giant magneto-resistive (GMR) heads to read and write data.

It is expected that for areal densities higher than 100 Gbit/in^2 the track density will increase at a higher rate than the linear bit density due to limitations in ultra-fast channel electronics. This will result in tighter TMR budgets, and will in turn impose a heavier burden on the servo control. One of the primary problems of servo control in hard disk drives is the presence of flexible structures between the voice coil motor (VCM) and

the head: the suspension, the E-block and the E-block pivot bearing. These flexible structures exhibit mechanical resonances that limit the closed-loop servo bandwidth.

The use of strain sensors for active vibration servo control in disk drives was proposed by several researchers [1, 2, 3] in order to increase the servo bandwidth. The basic idea was to strategically attach strain sensors to measure localized strains at key locations on drive structures, so that the sensors would effectively detect structural vibrations that may result in slider off-track vibration. The measured strain information can then be used in feedback control to damp out the resonances of those structure. In [1], a strain sensor was attached to the actuator and an external feedback control loop was used to actively damp the E-block resonances, especially the, so-called, butterfly mode. In [3], strain sensors were attached to the suspension, and the strain measurement was fed back in an inner loop to actively damp the suspension resonances. With the active feedback damping achieved in [1] and in [3], it was possible to design the servo controller to utilize a high open-loop gain to achieve a high closed-loop bandwidth.

In [4], CML proposed using the strain sensor measurement not only for active feedback control, but also for active feedforward compensation of suspension vibration. In [4], it was proposed that the strain measurements would provide real-time suspension vibration information that can be fed forward to compensate for TMR resulting from suspension vibration. The work is to be carried out on a piezoelectrically actuated dual-stage suspension as well as on a dual-stage suspension using a MEMS-type microactuator.

One of the main tasks in designing an instrumented suspension, for use in either of the control schemes described above, is determining the optimal location and orientation of the strain sensors in order to capture the dynamics of the desired modes: the modes that contribute significantly to the off-track motion of the slider. The subject of optimal sensor and actuator placement for flexible structures was treated by several researchers, for example [5] and [6]. Hac and Liu [6] proposed the use of some quantitative measure of the degree of observability of the modes under consideration in optimizing the sensor location. Huang et al [3], applied the concepts presented in [6] and used the observability gramian to determine the optimal location and orientation for a strain gauge on a suspension. However, the results obtained in [3] are not in agreement with expectations based on the modal strain field distributions in the suspension.

Krinke [2] presented an implementation of an instrumented suspension prototype. Four strain gauges were used in the prototype, and were arranged in a Wheatstone bridge circuit as shown in Fig. 1, in a configuration that would increase the sensitivity of the measurement. The configuration capitalized on the fact that certain high strain areas on the suspension are in opposite states of loading for the suspension off-track resonance modes, and it was designed to optimize the sensitivity of measuring the first torsion strains. The four sensor locations were determined by examining the strain distributions for the suspension first torsion, second torsion and sway modes, and selecting the regions exhibiting the highest levels of strain. The sensor orientations were selected as the principal strain angles of the strains generated by first torsion. The strain gauges used consisted of many deposited constantan elements that form a serpentine pattern at the

prescribed angle, as shown in Fig. 2, so as to increase the sensitivity of the strain measurement. The pattern was approximately 700 μm × 400 μm, with an element length of nearly 450 μm .

The objective of this study is to determine the optimal placement of strain sensors on a commercial suspension. The placement selection procedure is based on the theory presented in [6] and utilizes the minimum eigenvalue of the observability gramian as a quantitative measure of the degree of observability of the modes under consideration. Finite element analysis (FEA) is used to generate frequency response functions (FRFs) of the strain components in the plane of the suspension loadbeam at different locations. Modal analysis is then used to estimate the modal parameters of these FRFs, and a state space model, including the desired modes, is identified. The output matrix of the state space model is modified to include a strain projection matrix. A weighting matrix is also incorporated into the output matrix of the system to allow for assigning different weighting factors to the effect of the modes under consideration on the selection procedure. The weighting factors used are based on the modal contributions to slider off-track motion. The observability gramian is then computed and its eigenvalues are calculated at different locations and for different orientations on the loadbeam. The location/orientation combination that maximizes the minimum eigenvalue of the observability gramian is identified as the optimal combination for sensor placement. Since the eigenvalues of the observability gramian are related to the system output energy [6], maximizing the minimum eigenvalue ensures maximizing the output energy of the least observable state of the system, thus giving the best degree of observability.

2. Theory

A frequency response function $\alpha(s)$ can be expressed as the rational fraction of two polynomials, in the form

$$a(s) = \frac{\sum_{k=1}^{2n-2} b_k s^k}{\sum_{m=1}^{2n} a_m s^m} \quad (1),$$

where $s = i\omega$, ω is the frequency of excitation, and n is the number of active modes in the frequency range of the FRF. $\alpha(s)$ can be expressed as the modal summation

$$a(s) = \sum_{k=1}^{n} \frac{p_k \overline{w}_k s + q_k \overline{w}_k^2}{s^2 + 2z_k \overline{w}_k s + \overline{w}_k^2} \quad (2),$$

where $\overline{w}_k$ and z_k are the natural frequency and modal damping ratio, respectively, of the k^{th} natural mode.

The process of matching or curve-fitting a selected model of a structure to its frequency response data to determine the modal parameters of the structure is widely referred to as modal analysis. Many methods are available for modal analysis. The method employed in this study is a variation of the rational fraction polynomials (RFP) method [7], which is a multi-degree-of-freedom frequency-domain method.

A state space realization of the transfer function in Eq (2) is

$$\dot{\mathbf{x}} = \mathbf{A}\mathbf{x} + \mathbf{B}\mathbf{u} \quad (3),$$

with the output equation

$$\mathbf{y} = \mathbf{C}\mathbf{x} \tag{4},$$

where the matrices **A** and **B** are given by

$$\mathbf{A} = \begin{bmatrix} 0 & \overline{w}_1 & 0 & 0 & \dots & 0 & 0 \\ -\overline{w}_1 & -2z_1\overline{w}_1 & 0 & 0 & \dots & 0 & 0 \\ 0 & 0 & 0 & \overline{w}_2 & \dots & 0 & 0 \\ 0 & 0 & -\overline{w}_2 & -2z_2\overline{w}_2 & \dots & 0 & 0 \\ \vdots & \vdots & \vdots & \vdots & & \vdots & \vdots \\ 0 & 0 & 0 & 0 & \dots & 0 & \overline{w}_n \\ 0 & 0 & 0 & 0 & \dots & -\overline{w}_n & -2z_n\overline{w}_n \end{bmatrix} \tag{5},$$

$$\mathbf{B} = \begin{bmatrix} 0 & \overline{w}_1 & 0 & \overline{w}_2 & \cdots & 0 & \overline{w}_n \end{bmatrix}^T \tag{6},$$

and, for a single output system, **C** is given by

$$\mathbf{C} = \begin{bmatrix} p_1 & q_1 & p_2 & q_2 & \cdots & p_n & q_n \end{bmatrix} \tag{7}.$$

For a multi-output system with m outputs, **y** is an m×1 column vector, and the output matrix **C** is an m×n matrix of the form

$$\mathbf{C} = \begin{bmatrix} p_1^1 & q_1^1 & p_2^1 & q_2^1 & \cdots & p_n^1 & q_n^1 \\ p_1^2 & q_1^2 & p_2^2 & q_2^2 & \cdots & p_n^2 & q_n^2 \\ \vdots & \vdots & \vdots & \vdots & & \vdots & \vdots \\ p_1^m & q_1^m & p_2^m & q_2^m & \cdots & p_n^m & q_n^m \end{bmatrix} \tag{8}.$$

The vibration of the instrumented suspension is to be measured in terms of the strains generated by the suspension motion. The output of the strain gauge used depends upon both the location of the strain gauge and its orientation. Therefore, in the problem at hand, the system output of interest in identifying the optimal strain sensor placement is the strain ε projected in a given direction, identified by the angle θ from the x-axis. ε can

be computed once the plane strain components ε_x, ε_y, and γ_{xy} are known, according to Mohr's equation

$$e = \frac{e_x + e_y}{2} + \frac{e_x - e_y}{2}\cos 2q + \frac{e_{xy}}{2}\sin 2q \qquad (9),$$

where ε_x is the x-direction normal strain component, ε_y is the y-direction normal strain component, and γ_{xy} is the shear strain component. Eq. (9) can be expressed in matrix form as

$$e = \mathbf{C}_{\grave{e}}\mathbf{\mathring{a}} \qquad (10),$$

where

$$\mathbf{C}_{\grave{e}} = \begin{bmatrix} \frac{1+\cos 2q}{2} & \frac{1-\cos 2q}{2} & \frac{\sin 2q}{2} \end{bmatrix} \qquad (11),$$

and

$$\mathbf{\mathring{a}} = \begin{bmatrix} e_x \\ e_y \\ g_{xy} \end{bmatrix} \qquad (12).$$

The frequency range considered contains four active suspension modes: first torsion, sway, second torsion and third torsion. The FRFs of the strain components can therefore be expressed by Eq. (1) with n = 4. Thus, the state space formulation of the system has the form of Eq. (4) with **A** and **B** given by Eqs. (5) and (6), respectively, taking n = 4. An intermediate output matrix $\mathbf{C}_{\mathbf{int}}$ (with the three strain components as outputs) can be written, according to Eq. (8), and setting m = 3, as

$$\mathbf{C}_{\mathbf{int}} = \begin{bmatrix} p_1^x & q_1^x & p_2^x & q_2^x & p_3^x & q_3^x & p_4^x & q_4^x \\ p_1^y & q_1^y & p_2^y & q_2^y & p_3^y & q_3^y & p_4^y & q_4^y \\ p_1^{xy} & q_1^{xy} & p_2^{xy} & q_2^{xy} & p_3^{xy} & q_3^{xy} & p_4^{xy} & q_4^{xy} \end{bmatrix} \qquad (13).$$

The system output matrix is then given by

$$\mathbf{C} = \mathbf{C}_{\grave{e}}\mathbf{C}_{\mathbf{int}} \tag{14}$$

Structural conditions, such as controllability and observability play a vital role in the motion control of flexible structures. These conditions should not be violated by the arrangement of actuators and sensors on a structure, otherwise, control performance objectives may not be achieved. Of particular interest in this study is the observability condition, which is directly governed by the sensor placement. For example, the placement of a sensor near a nodal point of a mode will yield erroneous information about the contribution of that mode to the system response.

The observability gramian $\mathbf{W_o}$ of a system given by Eqs. (3) and (4) is defined by

$$\mathbf{W_o} = \int_0^\infty e^{\mathbf{A}^{\mathbf{T}}t}\mathbf{C}^{\mathbf{T}}\mathbf{C}e^{\mathbf{A}t}\,dt \tag{15}$$

If the observability gramian of a system is nonsingular, then the system is observable; if the observability gramian is singular, then the system is not observable. This binary character of the notion of observability renders it unsuitable for direct application to the problem of determining the optimal sensor placement. Hac and Liu [6] proposed a methodology for determining the optimal sensor placement in active motion control of flexible structures. The proposed approach uses the observability gramian of the system and relies on certain quantitative measures of its degree of observability. By noting that a system is considered to be completely observable if its observability

gramian is nonsingular, regardless of how close to being singular the gramian may come, Hac and Liu [6] suggested using the eigenvalues of the observability gramian as a measure of the degree of observability of the system.

A system with a nearly singular observability gramian (and equivalently, near-zero eigenvalues) is still strictly observable, but with a low degree of observability. In [6], it was demonstrated that the eigenvalues of the observability gramian are directly related to the output energy of the system. The smallest eigenvalue of the gramian corresponds to the output energy of the least observable state of the system. The optimal sensor placement is the one yielding the greatest minimum eigenvalue of the observability gramian, or equivalently, the least observable state with the greatest output energy. The proposed optimality criteria for the sensor placement provide a balance between the importance of the lower order and the higher order modes.

For flexible structures, a closed form solution for the observability gramian exists, and, for a continuous-time systems described by Eqs. (3) and (4), the gramian can be computed by solving the Lyapunov equation

$$\mathbf{A}^{\mathrm{T}}\mathbf{W}_{\mathbf{o}} + \mathbf{W}_{\mathbf{o}}\mathbf{A} + \mathbf{C}^{\mathrm{T}}\mathbf{C} = \mathbf{0} \qquad (16).$$

The existence of such a closed form solution renders the method computationally inexpensive, requiring only the determination of eigenvalues of the gramian at each step of optimization. Furthermore, the eigenvalues can be obtained in closed form when the structural damping is small and the natural frequencies are distinct and well spaced.

The system output matrix **C** can be further modified to account for the different contributions of the modes under consideration to slider off-track motion. **C** would then be given by

$$\mathbf{C} = \mathbf{C}_{\grave{e}}\mathbf{C}_{\mathbf{int}}\mathbf{C}_{w} \qquad (17),$$

where $\mathbf{C_w}$ is a weighting matrix that assigns a weighting factor to each of the modes.

The value of the amplitude of modal coordinate at its matching resonance is called the Q factor, or quality factor, of that mode[1]. The frequency points at which the magnitude of the modal coordinate falls to 0.707 of the quality factor of that mode are called the half power points of the mode, and the frequency band between these two points is called the bandwidth of the mode. In this study, the entries of $\mathbf{C_w}$ are based on the contribution of each mode to the slider off-track motion over the bandwidth of the mode.

3. Finite Element Modeling

This study was based on FEA simulations. The head gimbal assembly (HGA) model used for the Magnum 5E suspension consisted of the suspension loadbeam, the flexure, and the slider (Fig. 3). The loadbeam, the flexure, and the piezoelements were modeled using 5,686 SHELL181 4-node finite strain shell elements, with 6,387 nodes. The material propoerties used for the loadbeam and the flexure are those of stainless

[1] In analogy with some electrical engineering applications.

steel. They are listed, along with those used for the piezoelements, in Table 1. The flexure attachment to the loadbeam at the laser spot weld locations was modeled using BEAM4 3-D elastic beam elements. The flexure was also attached to the loadbeam at other locations using LINK8 3-D truss elements. The material used for the beam and link elements was assigned zero density and a high stiffness, so as to provide the desired attachment without dynamically loading the system. The loadbeam dimple was also modeled using LINK8 3-D truss elements. In order to model the point of contact between the dimple and the flexure, a node on the flexure coincident with the apex node of the dimple LINK8 elements was created, and the two nodes were constrained to have the same translational coordinates, but were allowed to rotate relative to each other.

The slider was modeled as a MASS21 structural mass element, which is a single-node element that can be assigned a mass and rotational mass moments of inertia. The mass element was given the following inertial properties, which are typical of a pico slider:

$m = 1.71\times10^{-6}$ kg

$I_{xx} = 0.141\times10^{-6}$ kg.mm^2

$I_{yy} = 0.221\times10^{-6}$ kg.mm^2

$I_{zz} = 0.\ 343\times10^{-6}$ kg.mm^2

The slider mass element was positioned at the location of the center of gravity of the slider and was attached to the flexure using BEAM4 3-D elastic beam elements. Air bearing dynamics were not considered in the modal and harmonic analyses since the air

bearing resonant frequencies are much higher than the frequency range considered. The slider was considered to have a fixed flying attitude: fixed flying height (z translational DOF), fixed pitch (y rotational DOF), and fixed roll (x rotational DOF).

4. Finite Element Analysis and Results

A modal analysis[2] was performed to compute the modal parameters of the suspension, and the suspension mode shapes were examined. The frequency range considered was 0-20 kHz. The natural frequencies and associated mode shapes of the suspension in this range are presented in Table 2.

A harmonic analysis[3] was then performed to obtain the FRFs of the slider motion and the three plane strain components (normal strain components ε_x, ε_y, and shear strain component γ_{xy}) in all elements on the loadbeam to a unit lateral excitation at the baseplate area. The 0-20 kHz frequency range contained four active suspension modes: first torsion, sway, second torsion and third torsion. These modes are depicted in Fig. 4. Figure 5 shows the FRF of the slider off-track response to a unit lateral excitation at the baseplate area. The response plotted is the slider motion relative to the baseplate motion. Figures 7, 8, and 9 show sample strain FRFs for the strain components ε_x, ε_y, and γ_{xy}, respectively, at five arbitrary elements (marked in Fig. 6). The vertical scale on these

[2] A modal analysis in ANSYS identifies the natural frequencies and mode shapes of the structure.
[3] A modal analysis in ANSYS determines the response of the structure (as a complex quantity) to sinusoidally varying loads applied at selected nodes (in the form of displacements or forces).

plots is the decibel of the absolute value of each FRF (which is generally a complex quantity), with the reference taken as 1 unit. It should be noted that a damping ratio of 0.0013 was imposed during the harmonic analysis in ANSYS. This value is an estimate of the average modal damping ratio based on unpublished experimental results.

An examination of the strain intensity distributions corresponding to the four active natural modes indicated that the bend area and the central region between the bend area and the baseplate area exhibit the highest level of strain for all four modes. Close-up views of the strain intensity distributions around these areas for the four modes are given in Fig. 10. Blue and red indicate the lowest and highest levels, respectively, of strain intensity in the contour color scale to the right of Fig. 10. It should be noted that the four distributions have different scales: a comparison of strain levels across the different modes is meaningless.

The modified RFP method used for modal analysis was coded in MATLAB, and the modal parameters (natural frequencies, modal damping factors, and modal residues) associated with each strain FRF were computed for each element on the suspension loadbeam. The computed parameters were then used in building the system matrices as given by Eqs. (5), (6), and (13).

5. Optimization Results

After constructing the system matrices at each element on the loadbeam, the strain was projected at angles in increments of 1° at each of these elements. The observability gramian and its eigenvalues were then computed for each element and strain projection angle combination according to Eqs. (15) and (16). The element and projection angle combination yielding the greatest minimum eigenvalue was identified as the optimal sensor placement. The entire procedure was carried out twice using MATLAB. In the first run, the output matrix given by Eq. (14) was used, so that the weighting matrix $\mathbf{C_w}$ is the identity matrix, and all modes are assigned an equal relevance in the selection procedure. In the second run, the output matrix given by Eq. (17) was used, where the entries of the weighting matrix $\mathbf{C_w}$ were calculated based on the contribution of each mode to the slider off-track motion over the bandwidth of the mode.

The optimal sensor placement for the first case where $\mathbf{C_w} = \mathbf{I}$ was at element 559, at an angle of 92°, as shown in Fig. 11. However, the results presented in Fig. 11 may not be very practical due to the small size of the selected element. On average, the element dimensions in the bend area are approximately 100 μm in the x-direction by 75 μm in the y-direction, whereas target dimensions for implementing an instrumented suspension at CML are 100 μm × 225 μm, or, equivalently, a three-element strip: one element long in the x-direction and three elements long in the y-direction. In order to provide more applicable results, it was necessary to identify larger regions at which the minimum gramian eigenvalues assumed the highest values for certain directions. There were four

such regions, as depicted in Fig. 12. Red represents the highest gramian minimum eigenvalue level in the color scale in the figure.

The orientation of the strain sensor in each element strip was based on the average minimum eigenvalue of the three elements in the strip. The strain projection angle yielding the highest average minimum eigenvalue was identified as the optimal sensor orientation at the corresponding element strip. Figure 12 indicates the optimal projection angle for each of the selected regions, and Table 3 lists the associated average minimum eigenvalues. Region R1 represents the best location for a single strain sensor. However, the degrees of observability at regions R2, R3, and R4 are only slightly lower than that at R1, and strain sensor placement at any of these regions (with the specified orientation) is expected to yield comparable results to those obtained using region R1.

The results presented in Fig. 12 are especially useful for implementations of the instrumented suspension similar to that presented in [2], in which four strain gauges are arranged in a Wheatstone bridge circuit, in a configuration that would increase the sensitivity of the measurement. Such a configuration utilizes the fact that two pairs of regions are in opposite states of loading for all modes: pair R1-R4 is in tension (compression) during the time pair R2-R3 is in compression (tension) for the three torsion modes; and pair R1-R3 is in tension (compression) during the time pair R2-R4 is in compression (tension) in the sway mode. For the Magnum 5E suspension, sway is the major contributor to slider off-track motion, which suggests using a Wheatstone configuration that would maximize the measurement sensitivity to the sway mode. Figure

13 illustrates the variation of the average minimum eigenvalues as a function of the strain projection angle in the four regions of Fig. 12.

The entries of $\mathbf{C_w}$ for the second case were determined based on the slider off-track frequency response presented in Fig. 5. The normalized modal TMR contributions used as weighting factors are listed in Table 4. The optimal sensor placement for this case was at element 559, at an angle of 92°, as shown in Fig. 11. Note that this result is identical to that obtained using $\mathbf{C_w} = \mathbf{I}$. The four three-element strips at which the minimum gramian eigenvalues assumed the highest values for certain directions are identified in Fig. 14. The optimal orientation of the strain sensors for these element strips was based on the average minimum eigenvalue of the three elements in the strip. Figure 14 indicates the optimal projection angle for each of the selected regions, and Table 5 lists the associated average minimum eigenvalues. Once again, region R1 represents the best location for a single strain sensor. Figure 15 illustrates the variation of the average minimum eigenvalues as a function of the strain projection angle in the four regions of Fig. 14.

6. Conclusion

The objective of this study was to determine the optimal placement of strain sensors on a commercial suspension. The optimal placement selection procedure was based on maximizing the degree of observability of the suspension first torsion, sway, second torsion and third torsion modes, which are the modes that contribute to off-track motion. The minimum eigenvalue of the observability gramian was used as a quantitative measure of the degree of observability of these modes.

The optimal sensor location and orientation on the suspension loadbeam were identified for two cases: in the first, equal weighting factors were assigned to all modes; in the second, weighting factors based on the modal TMR contributions were assigned to the modes. Both cases yielded the same result. In addition, the four locations on the suspension loadbeam with the highest degree of observability of the selected modes were identified for implementations of the instrumented suspension in which four strain gauges are arranged in a Wheatstone bridge circuit, in a configuration that would increase the sensitivity of the measurement. The results obtained for the two cases described above were nearly identical.

7. References

1. Huang, F. Y., Imaino, W., Semba, T., Lee, F., "Rotary Actuator Dynamics With Active Damping," 11th Annual Symposium on Information Storage and Processing Systems, Session 8: HDD Actuator Design/Dynamics, June 1999.
2. Krinke, T. A., "Second Generation Namakan Suspension," Technical Report, Hutchinson Technology, Inc., November 1998.
3. Huang, Y., Banther, M., Mathur, P. D., Messner, W. C., "Design And Analysis Of A High Bandwidth Disk Drive Servo System Using An Instrumented Suspension," IEEE/ASME Transactions on Mechatronics, Vol. 4, No. 2, June 1999.
4. Li, Y., and Horowitz, R., "Characterization And Compensation Of Air Turbulence Induced Vibration With Dual-Stage Actuators," 12th Annual Computer Mechanics Laboratory Sponsors Meeting, January 2000.
5. Lim, K. B., "Method For Optimal Actuator And Sensor Placement For Large Flexible Structures," Journal of Guidance, Control and Dynamics, Vol. 15, No. 1, pp. 49-57, January-February, 1992.
6. Hac, A., and Liu, L., "Sensor And Actuator Location In Motion Control Of Flexible Structures," Journal of Sound and Vibration, Vol. 167, No. 2, pp. 239-261, 1993.
7. Ewins, D. J., "Modal Testing: Theory, Practice and Application," Hertfordshire, England: Research Studies Press Ltd., 2000.

Acknowledgements

This study was supported by the Computer Mechanics Laboratory at the University of California at Berkeley. The authors would like to thank Robert Evans of Hutchinson Technology Inc. for providing suspension samples and a starting finite element model of the Magnum 5E suspension. Special thanks go to Todd Krinke of Hutchinson Technology Inc. for sharing information on work carried out at Hutchinson on implementations of the instrumented suspension.

Material	*Young's Modulus [GPa]*	*Shear Modulus [GPa]*	*Density [kg/m³]*	*Poisson's Ratio*
Stainless Steel	180	68.182	8072	0.32
Piezo-element material	62	23.485	7800	0.32
LINK8 and BEAM4 material	280	80	0	0.32

Table 1: Material properties used in the finite element model.

Mode	*Frequency [Hz]*	*Mode Shape*
1	2732	First bending
2	5418	Second bending
3	6737	First torsion
4	8635	Sway
5	9329	Flexure torsion
6	9639	Third bending
7	10918	Flexure bending
8	12118	Second torsion
9	14644	Flexure bending
10	14952	Fourth bending
11	15739	Third torsion
12	18315	Flexure bending

Table 2: Natural frequencies and associated mode shapes of the Magnum 5E suspension.

Region	*Projection Angle*	*Average Minimum Eigenvalue*
R1	91°	22.423×10^{-9}
R2	89°	22.175×10^{-9}
R3	86°	19.863×10^{-9}
R4	94°	19.607×10^{-9}

Table 3: Optimal strain projection angles and corresponding average minimum eigenvalues for the four regions shown in Fig. 12 ($\mathbf{C}_w = \mathbf{I}$).

Mode	*Weighting Factor*
T1	0.0167
S	0.9129
T2	0.0593
T3	0.0111

Table 4: Normalized modal TMR contributions used as weighting factors in $\mathbf{C_w}$ for the case $\mathbf{C_w} \neq \mathbf{I}$.

Region	*Projection Angle*	*Average Minimum Eigenvalue*
R1	91°	27.430×10^{-13}
R2	89°	27.127×10^{-13}
R3	88°	24.881×10^{-13}
R4	92°	24.473×10^{-13}

Table 5: Optimal strain projection angles and corresponding average minimum eigenvalues for the four regions shown in Fig. 14 ($\mathbf{C_w} \neq \mathbf{I}$).

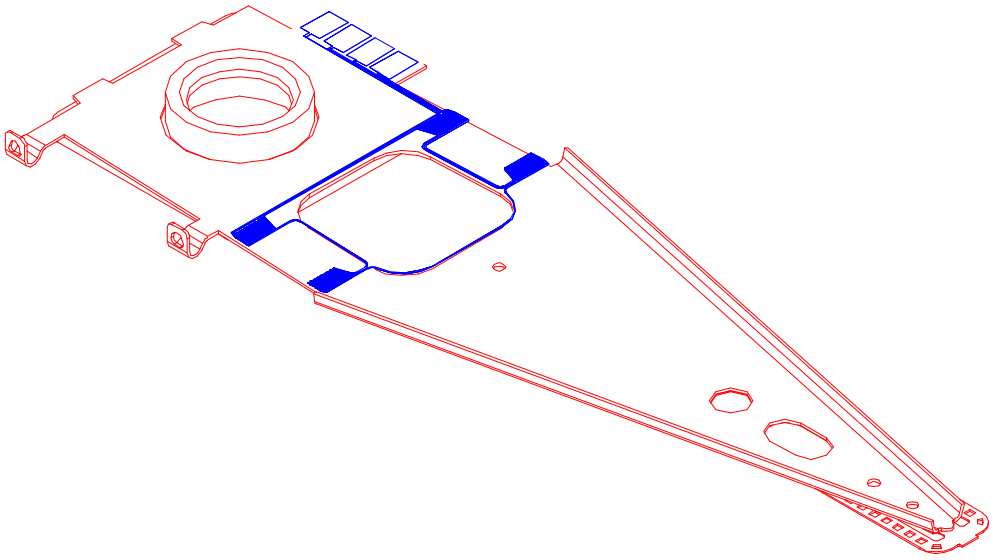

Figure 1: Full Wheatstone bridge strain gauge configuration*.

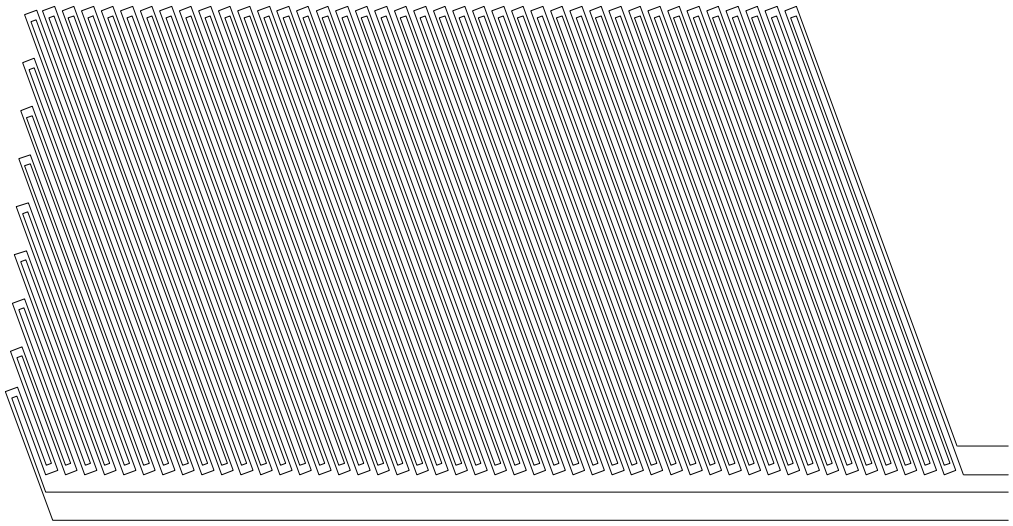

Figure 2: Strain gauge consisting of serpentine pattern of constantan elements*.

* Figure courtesy of Todd Krinke, Hutchinson Technology Inc.
* Figure courtesy of Todd Krinke, Hutchinson Technology Inc.

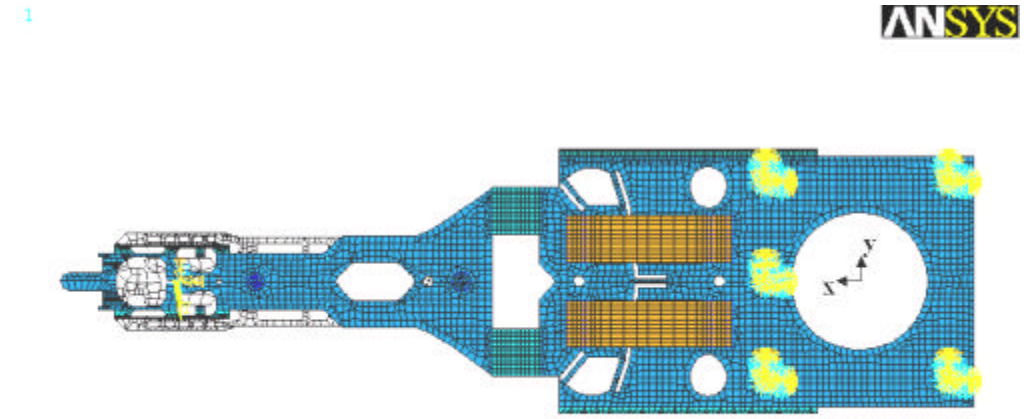

Figure 3: FE model of the Magnum 5E suspension.

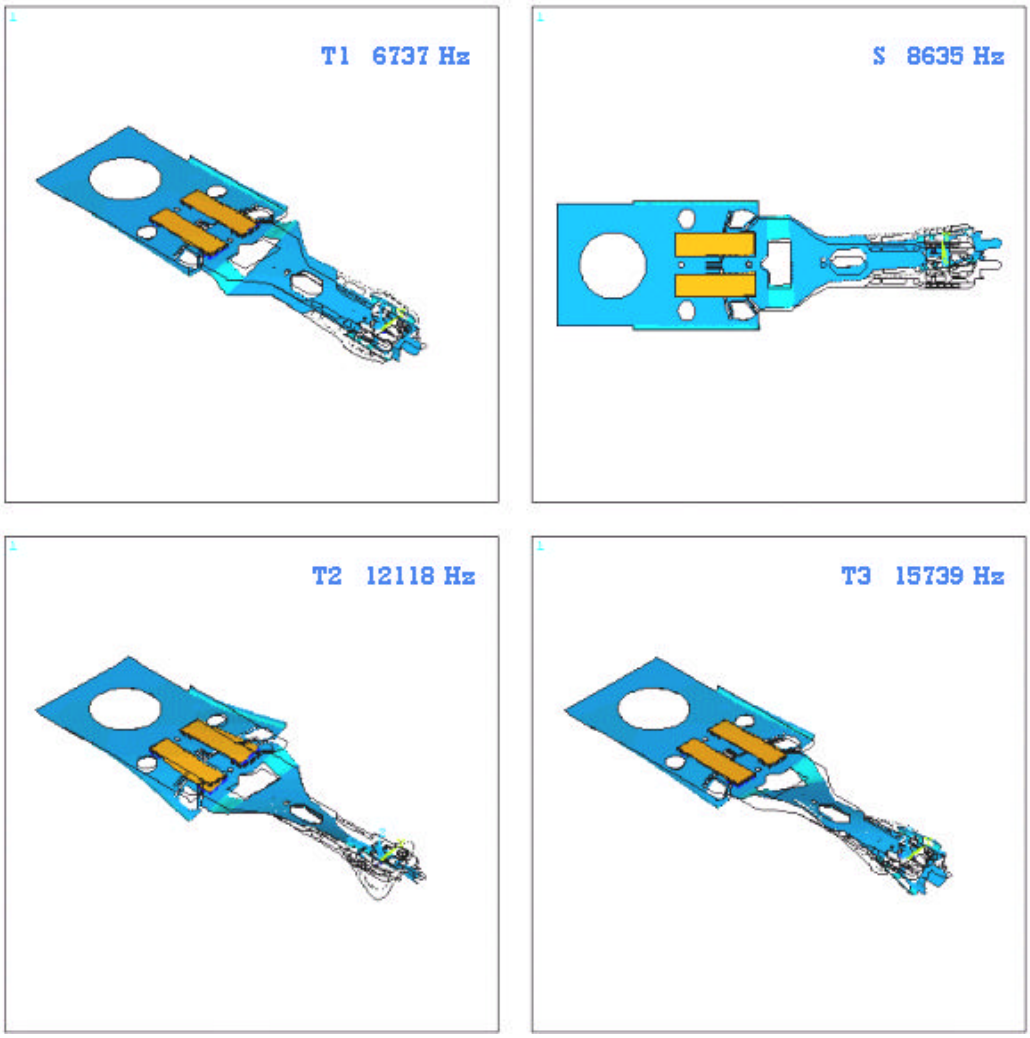

Figure 4: Suspension first torsion (T1), sway (S),
second torsion (T2), and third torsion (T3).

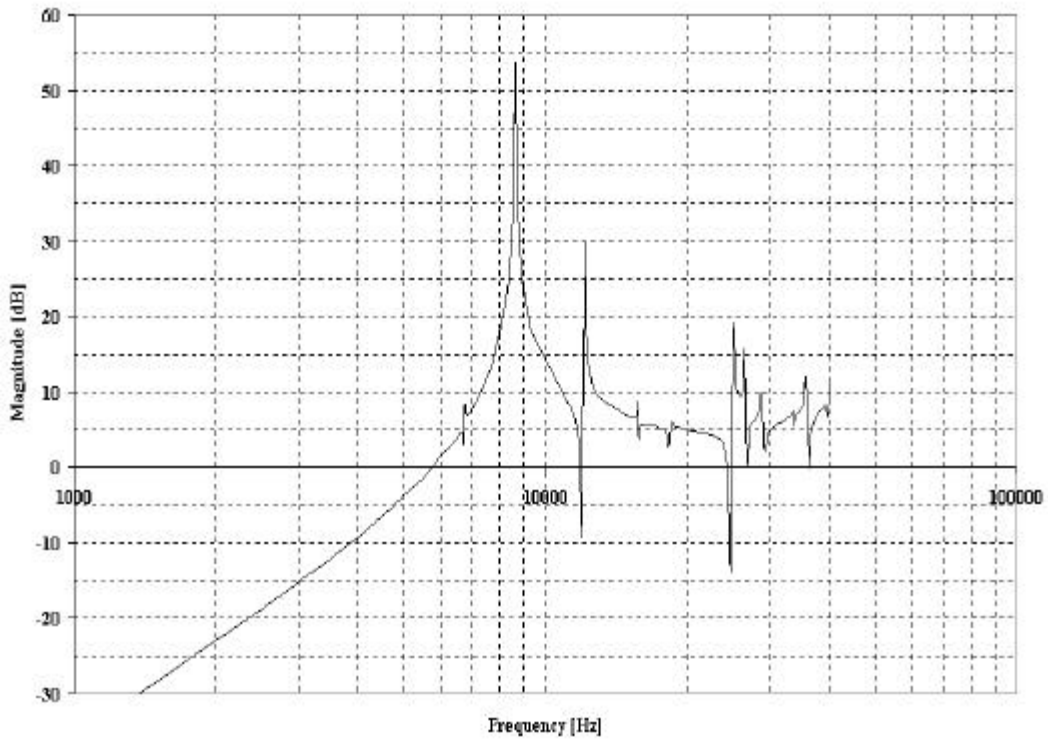

Figure 5: FRF of slider off-track response to a unit lateral excitation at the baseplate area.

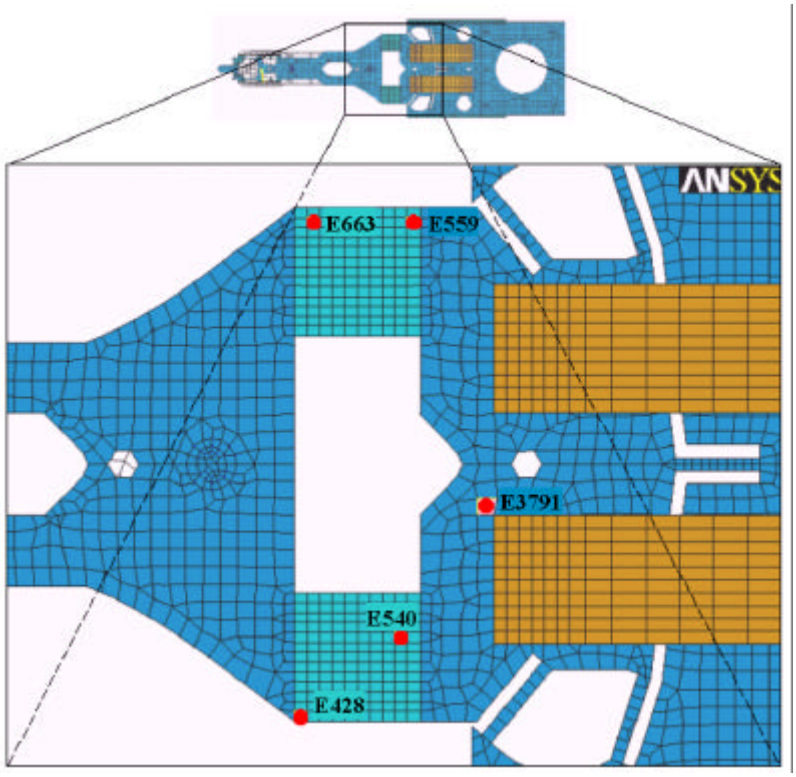

Figure 6: Close-up of the central region on the suspension, and positions of five arbitrary elements for strain component FRF samples.

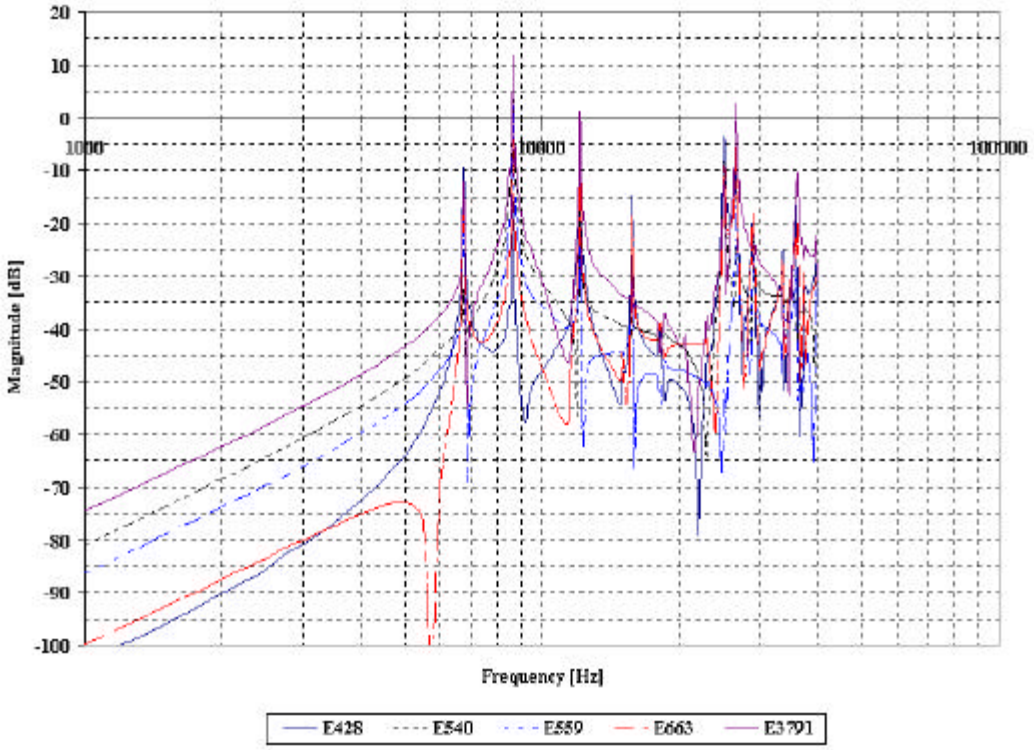

Figure 7: FRFs of normal strain component ε_x response at five arbitrary elements to a unit lateral excitation at the baseplate area.

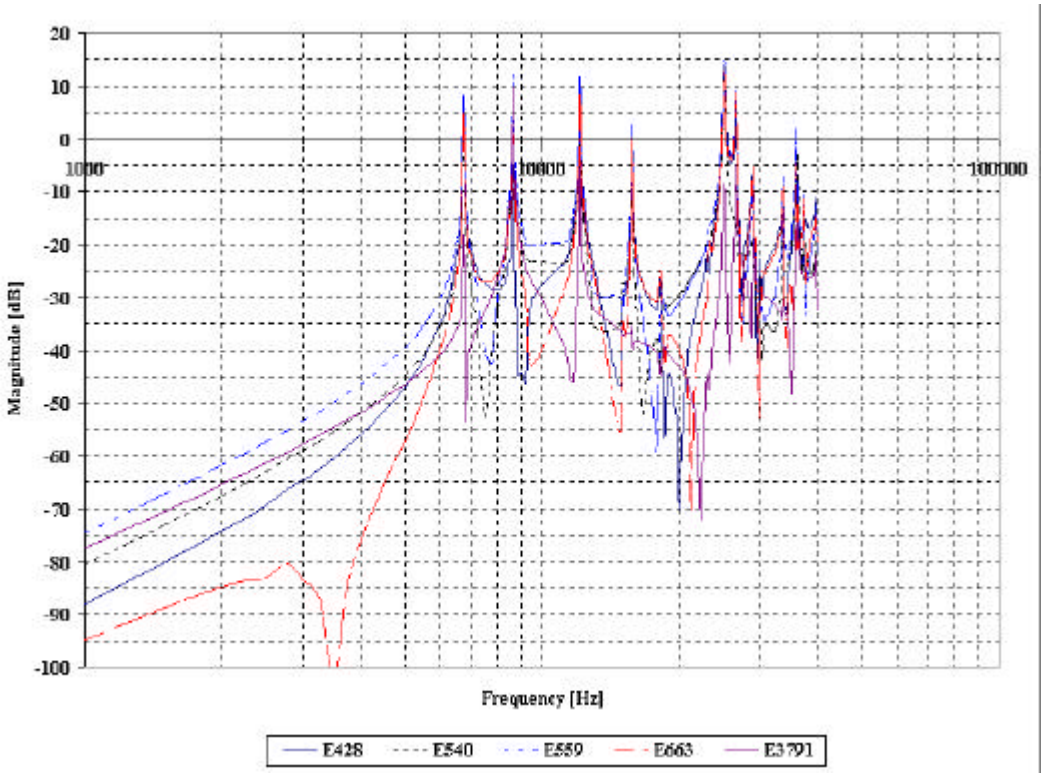

Figure 8: FRFs of normal strain component ε_y response at five arbitrary elements to a unit lateral excitation at the baseplate area.

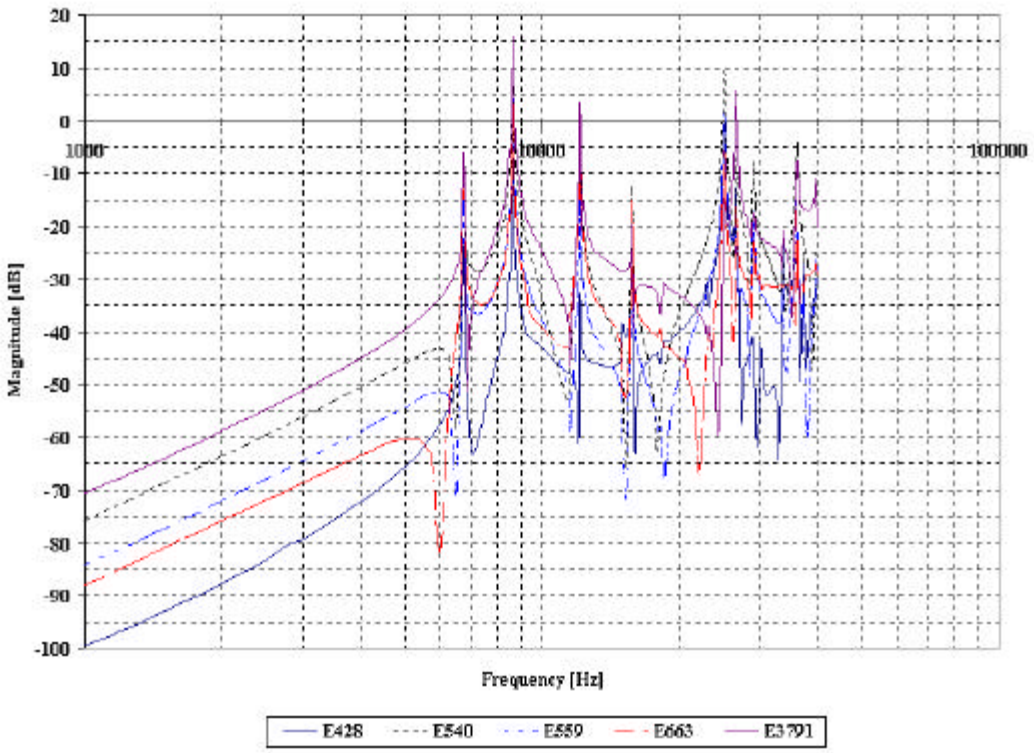

Figure 9: FRFs of shear strain component γ_{xy} response at five arbitrary elements to a unit lateral excitation at the baseplate area.

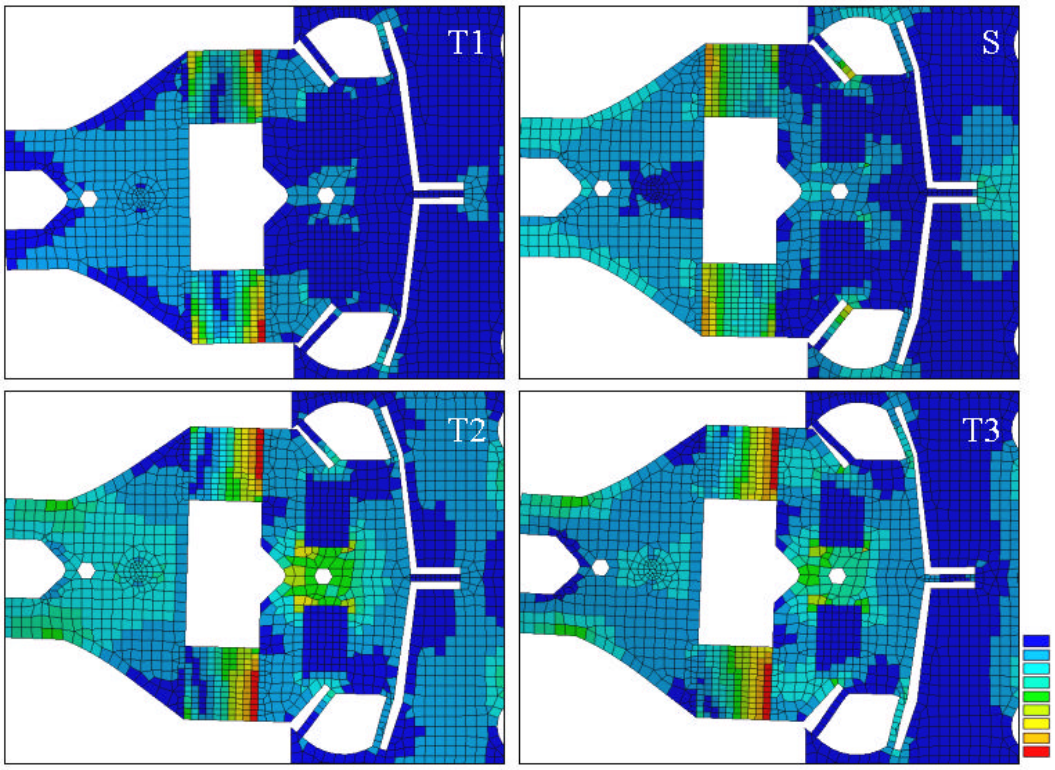

Figure 10: Strain intensity distributions in suspension first torsion (T1), sway (S), second torsion (T2), and third torsion (T3).

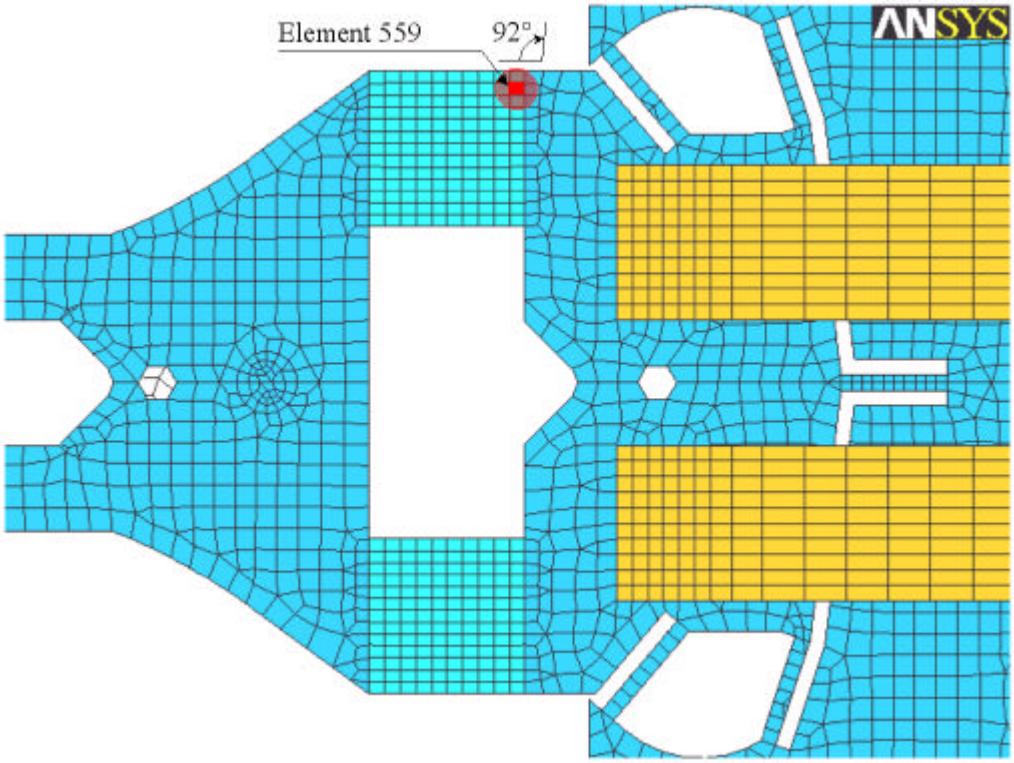

Figure 11: Optimal sensor placement for $\mathbf{C_w} = \mathbf{I}$, and for $\mathbf{C_w} \neq \mathbf{I}$.

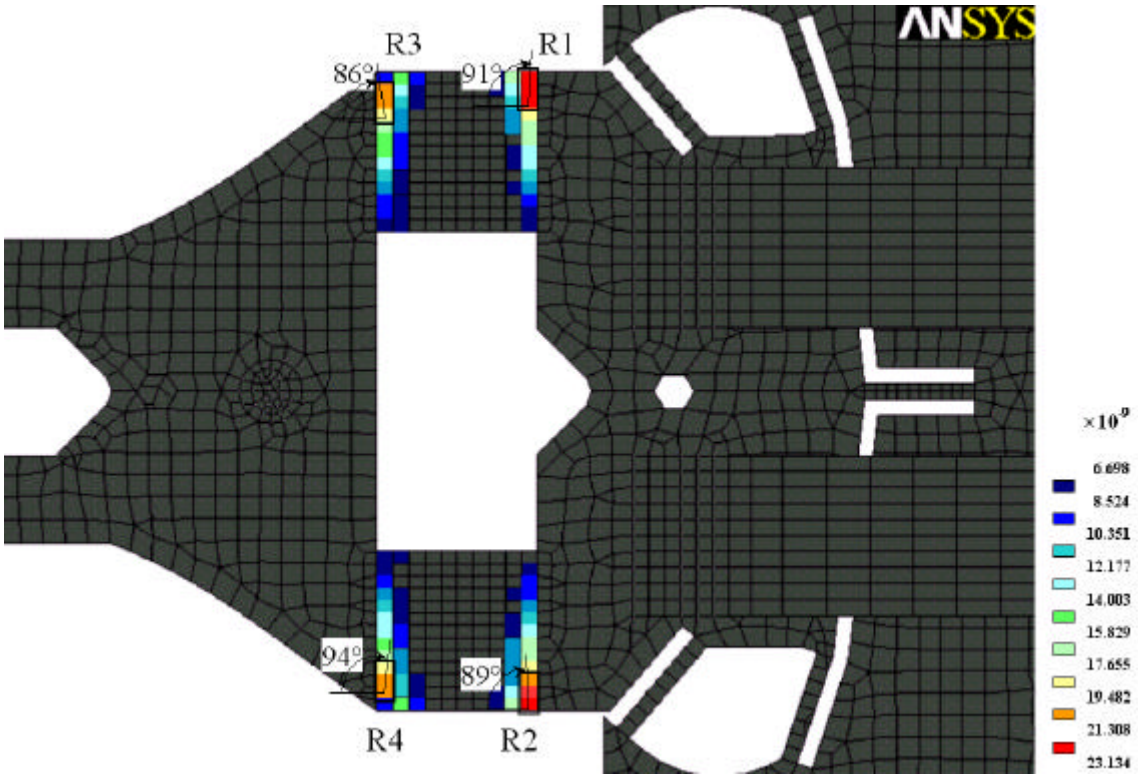

Figure 12: Regions with the highest minimum eigenvalues for $\mathbf{C_w} = \mathbf{I}$.

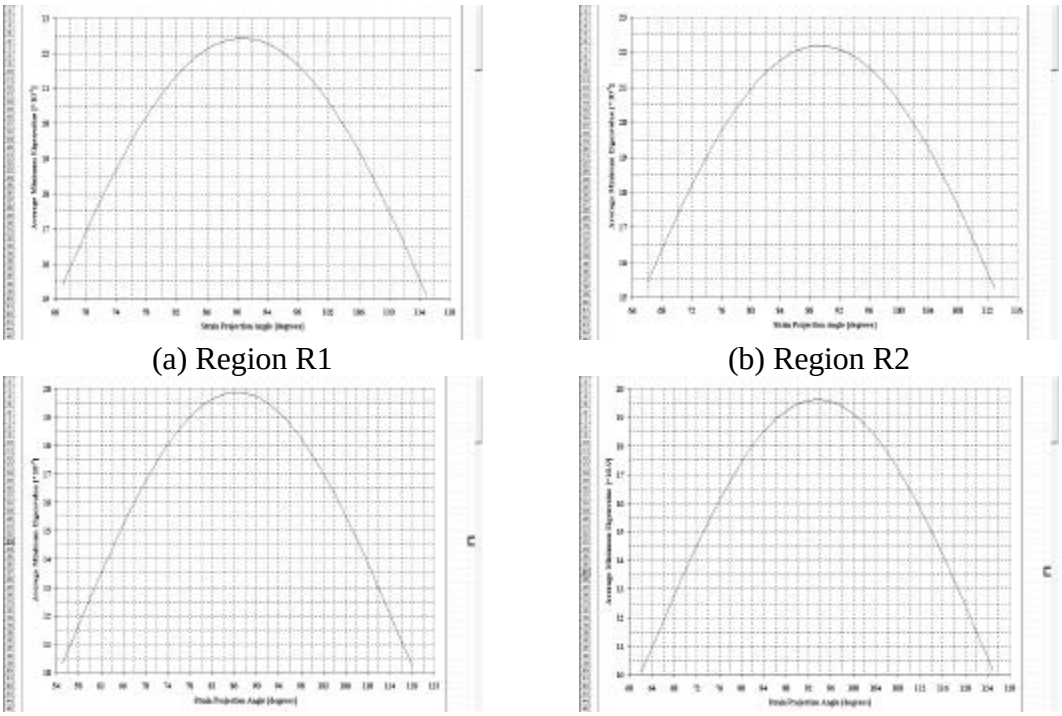

(a) Region R1 (b) Region R2

(c) Region R3 (d) Region R4

Figure 13: Variation of the average minimum eigenvalues as a function of the strain projection angle in the four regions of Fig. 10.

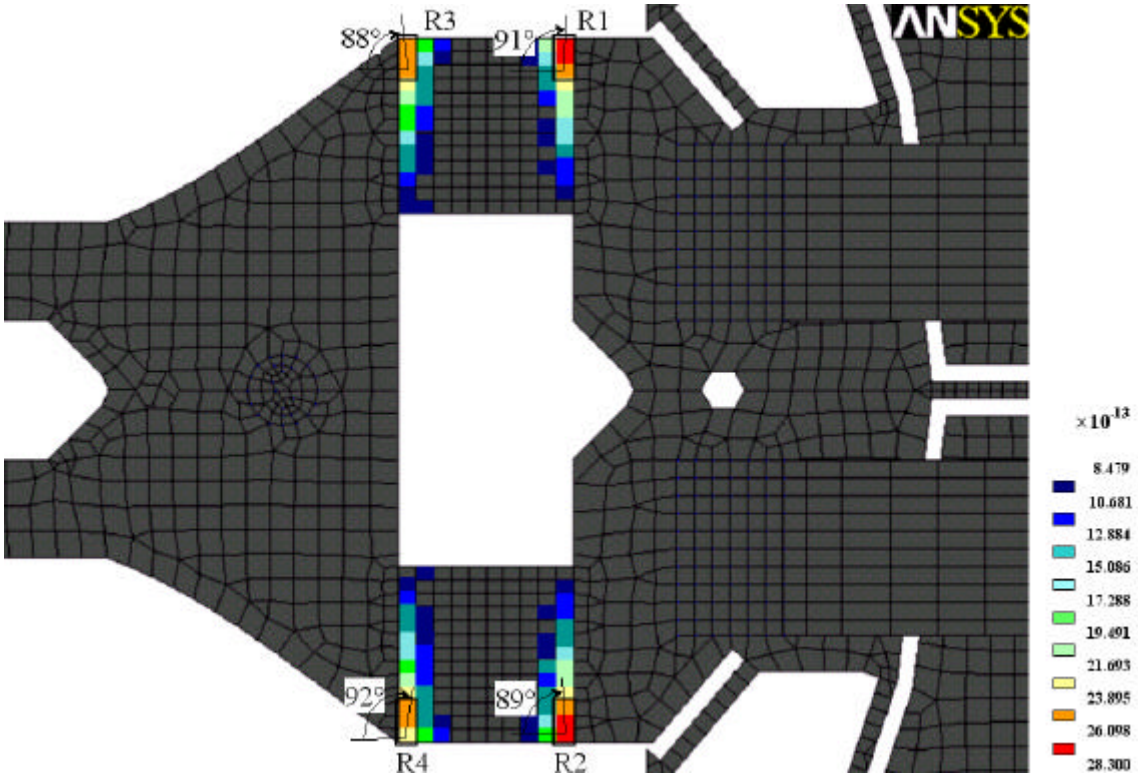

Figure 14: Regions with the highest minimum eigenvalues for $\mathbf{C_w}$ based on modal contribution to TMR.

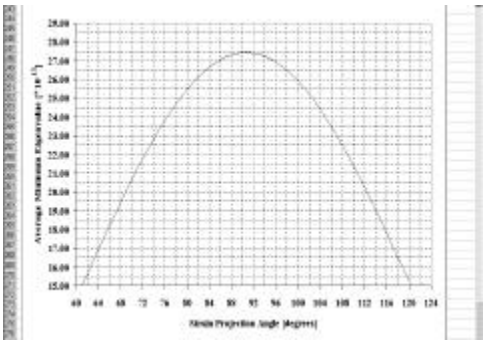

(a) Region R1

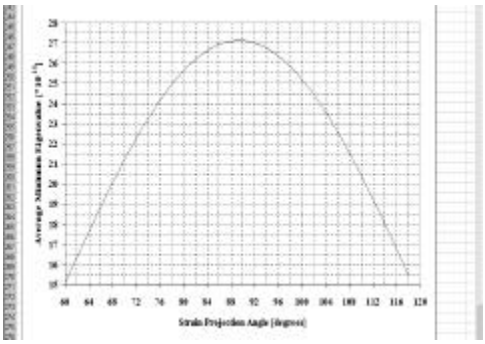

(b) Region R2

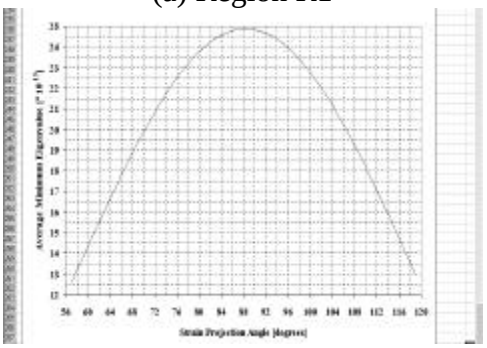

(c) Region R3

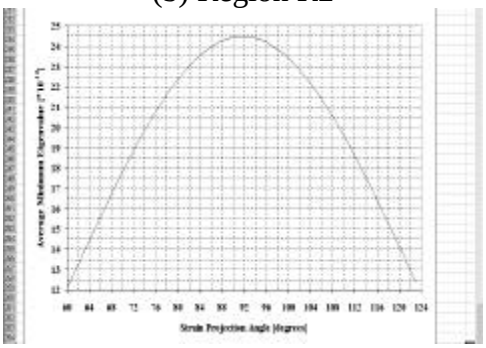

(d) Region R4

Figure 15: Variation of the average minimum eigenvalues as a function of the strain projection angle in the four regions of Fig. 12.